Bulletin of Volcanology (2023) 85:40
https://doi.org/10.1007/s00445-023-01653-0

RESEARCH ARTICLE

Late Holocene edifice collapse and eruptions of Iriga volcano, Philippines: integrated data from subaerial and lacustrine deposits

Alexander Belousov[1] · Marina Belousova[1] · Eddie Listanco[2]

Received: 19 November 2022 / Accepted: 25 May 2023

Abstract
Mount Iriga is a small, dormant stratovolcano of basalt to basaltic andesite composition located in Luzon Island, Philippines. The volcanic edifice includes a well-preserved horseshoe-shaped avalanche scar 2 km across with an adjacent fan of hummocky debris avalanche deposit (DAD) formed by large-scale (1.5 km^3) gravitational edifice collapse. To constrain the age of the collapse and determine the character of volcanic activity that followed, we investigated and dated (using the ^{14}C accelerator mass spectrometry method) paleosoils and organic lake sediments as well as charcoal-containing pyroclastic deposits that closely pre- and post-dated emplacement of the DAD. We found that the collapse of Iriga occurred soon after its 1830 ± 40 BP explosive magmatic eruption (of St. Vincent type) that produced pyroclastic flows of scoriaceous basaltic andesite. In the avalanche-dammed Lake Buhi, the organic bottom sediments started to accumulate at 1780 ± 30 BP, marking the upper age limit of the DAD emplacement. The edifice collapse itself was not contemporaneous with any geologically detectable explosive eruption. After the collapse, a stubby block lava flow with volume of about 0.02 km^3 was extruded inside the horseshoe-shaped avalanche scar. The next eruption of Iriga, which was its only post-collapse explosive eruption, occurred at 1110 ± 30 BP. This phreatomagmatic eruption left a small steep-walled maar-like crater inside the broad avalanche scar in the vent area of the block lava flow. The extrusion of the block lava and the subsequent phreatomagmatic event were the only eruptions of Iriga that occurred after the edifice collapse. Together with the pre-collapse explosive eruption, they comprise the entire eruptive activity of Iriga during the Late Holocene and all occurred during the last 2000 years.

Keywords Mount Iriga · Large-scale volcanic collapse · Debris avalanche · Eruption · Pyroclastic deposits · Radiocarbon dating · Coring of lake sediments

Introduction

Since the 1980 eruption of Mount St. Helens, USA, it has been established that volcanic edifices are gravitationally unstable and prone to large-scale collapses with generation of long-runout debris avalanches (Voight et al. 1981; Siebert 1984). Such collapses result in formation of distinctive avalanche scars with characteristic horseshoe-shaped morphologies and corresponding debris avalanche deposits (DADs) with hummocky surface topographies (Ui 1983; Glicken 1996). Both the avalanche scars and the DADs have distinctive morphological features with excellent preservation potential, making them easily recognizable even after many thousands of years. Globally, several hundred DADs formed by large-scale (volumes > 0.1 km^3) volcanic collapses have been identified as have occurred during the Holocene (Dufresne et al. 2021). In fact, large-scale collapses are rather common events and can occur on a volcano of almost any type, where some volcanoes have experienced multiple collapses (Beget and Kienle 1992; Belousov et al. 1999; Siebert and Roverato 2021). Analysis of multiple prehistoric, as well as several historical cases, has shown that they can be triggered by a number of natural causes from heavy rain events to tectonic earthquakes (Delcamp et al. 2016; Siebert 1984). However, the most common cause is shallow level intrusion of magma (Belousov et al. 2007). Large-scale collapses abruptly reduce lithostatic pressure on the magma feeding system of the collapsing volcano and shorten the length of the volcanic conduit. Jointly these effects lead to intensification of the volcano's activity, both

Editorial responsibility: J. Fierstein

Alexander Belousov
belousov@mail.ru

[1] Institute of Volcanology and Seismology, Petropavlovsk-Kamchatsky, Russia

[2] Daraga, Albay, Philippines

Published online: 04 June 2023

immediately after the collapse and over a longer time scale (Watt 2019). The primary factors determining the character of post-collapse eruptions are the depth of the intruding magma inside the edifice in the moment of failure and the relative positions of the intrusion and the detachment surface (Belousov et al. 2007). Thus, it can be assumed that an edifice collapse event naturally probes the condition of the shallow magma system at the moment of the collapse (Eichelberger 2006). Types and magnitudes of eruptions that follow large-scale collapses cover a very broad spectrum and vary from magmatic to non-magmatic (hydrothermal) as well as from highly explosive (directed blasts and/or Plinian activity) to quiet extrusive (lava flow or dome forming) (Siebert 1984).

Seven historic cases of large-scale volcanic collapses are known globally: Bandai 1888, Harimkotan 1933, Lamington 1951, Bezymianny 1956, Shiveluch 1964, Mount St. Helens 1980, and Soufriere Hills, Montserrat 1997 (Nakamura and Glicken 1988; Belousov et al. 2007; Belousov et al. 2020). Direct observations of these events have provided the most comprehensive data about collapse-related eruptive activity. However, such observations are rare. Hence, geological investigations of prehistoric collapses, especially relatively young ones, provide most of the data we have regarding eruptive activity associated with large-scale collapses. In these cases the collapse-related eruptive activity is recorded in stratigraphic sequences as layers of pyroclasts and/or lava flows synchronous with, and/or closely postdating, the collapse. Characteristics of such deposits can be interpreted in terms of the types and mechanisms of the parental eruptions. In addition, C^{14} dating, combined with stratigraphic interrelations between layers, permits reconstruction of the timing and sequence of the eruptive events and their link to the large-scale collapses.

To add further to our understanding of the relationship between large-scale collapses and the activity they trigger, we thus focus on the Holocene case of Mount Iriga, Philippines. We use stratigraphic relations between volcaniclastic deposits supported by radiocarbon dating to draw the link between the collapse event and eruptions that preceded and followed.

Geological setting

Iriga volcano

Mount Iriga (Global Volcanism Program https://volcano.si.edu/volcano.cfm?vn=273041), locally known as Mt. Asog, is a small (1196 m asl), long-dormant stratovolcano located in the southeastern part of Luzon Island, Philippines. Structurally, Iriga is located on the Bicol Volcanic Arc at the central-eastern margin of the Philippine Mobile Belt (Fig. 1).

The volcanic edifice is mostly of basalt to basaltic andesite composition with some andesites and dacites (Aguila 1986; duFrane et al. 2006). The edifice has a well-preserved, deeply incised horseshoe-shaped avalanche scar 2 km across (Fig. 2). Inside this scar there are two younger volcanic landforms: a thick lava flow and small inner crater (Fig. 3).

The avalanche scar opens southeastward where there is a broad fan of hummocky DAD (Fig. 4) extending from it. Based on reports of missionaries, it was supposed that Mount Iriga collapsed and erupted in 1628, and subsequently produced no eruptions (Aguila 1986). Emplacement of the DAD dammed the broad valley of the Barit River and led to the formation of large Buhi Lake, which has dimensions of 6×4 km and a depth of up to 18 m. We name this DAD "Buhi DAD" to distinguish it from another, much older, DAD of Iriga (Paguican et al. 2012). In addition, we call the corresponding horseshoe-shaped scar "Buhi avalanche scar" and the collapse itself the "Buhi collapse."

Our main target is to constrain the age of the Buhi collapse and to determine the ages and styles of the post-collapse eruptions.

Buhi debris avalanche

Buhi DAD covers an area of 70 km^2 at the SE foot of the volcano (Fig. 4) with an average thickness of 20–25 m. The volume of the deposit is estimated to be 1.5 km^3, which is about 10% of the volume of the former volcanic edifice (Aguila 1986). The height of the Iriga edifice (H) before the Buhi collapse was about 1.3 km above the volcano's base, i.e., its ring plane (Paguican et al. 2012). Hence, the runout distance (L) of Buhi debris avalanche is 11 km, so that the apparent friction coefficient (H/L) is 0.114 (calculated by Yoshida 2013). The deposit has a hummocky surface typical of DADs. Several exceptionally large hummocks up to 500 m across and 50 m high are located in the axial zone of the avalanche at a distance of 1–4 km from the source (Fig. 2). These are probably toreva blocks—relatively intact sliding blocks of the Buhi collapse that were not incorporated into the debris avalanche, and came to rest in the proximal zone (Paguican et al. 2012). Average size of the avalanche hummocks decreases with distance from the volcano (Yoshida 2013).

Most of the hummocks are composed of block facies (terminology from Glicken 1996) represented by fragments of strongly brecciated lava flows of the collapsed part of the edifice. A significant part of the avalanche deposit is composed of entrained material of the avalanche substrate which is represented by volcaniclastic deposits (former deposits of pyroclastic flows, lahars, and alluvium of the ring plane) (Paguican et al. 2012). These deposits were bulldozed by the avalanche and incorporated into the avalanche during its motion and deposition (bulldozer facies after Belousov et al. 1999).

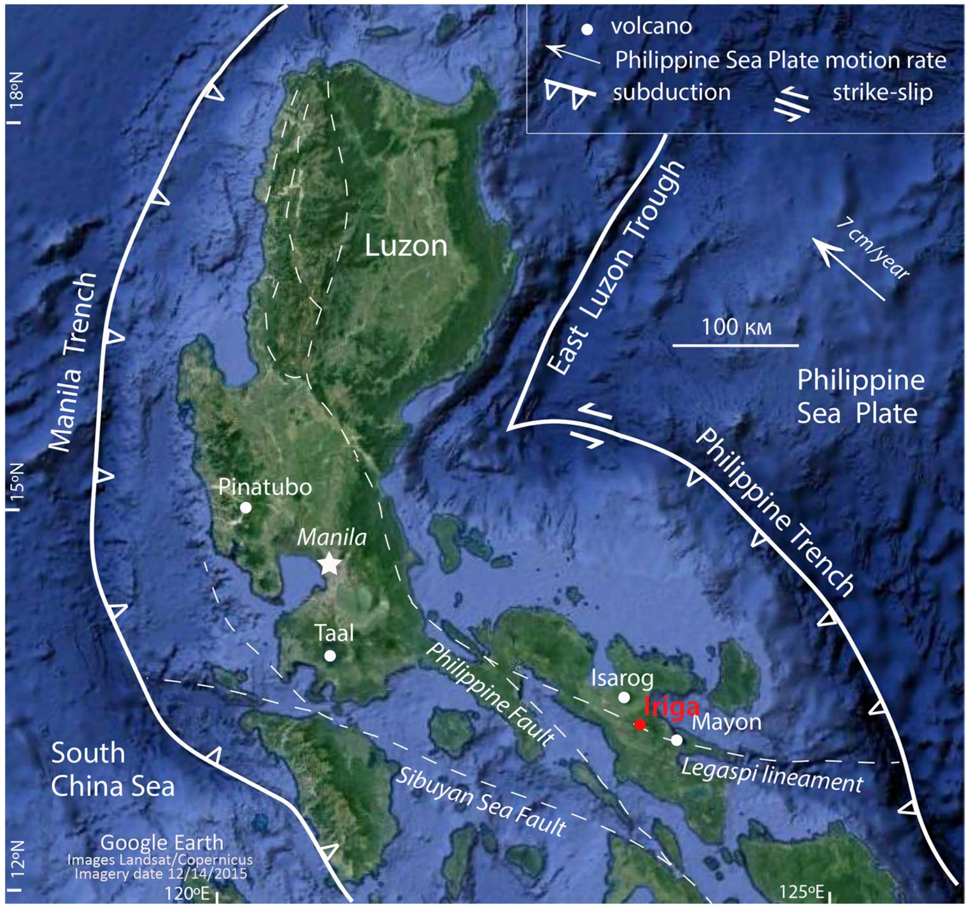

Fig. 1 Tectonic framework of Iriga volcano (modified from Pasquaré and Tibaldi 2003)

Fig. 2 Iriga volcano with horseshoe-shaped avalanche scar and large hummocks of Buhi debris avalance deposits, up to 50 m high, in the foreground. View from SE

The two most common substrate deposits entrained into the Buhi debris avalanche are light-gray silica-rich pumice PF (Fig. 5a) and gray to dark-gray PFs of scoriaceous basaltic andesite related to a St. Vincent-type eruption predating DAD (Aguila 1986) (Fig. 5b).

Methodology

The sequence of eruptive events that followed Buhi edifice collapse was reconstructed using geomorphologic analysis of the volcanic edifice, focusing on spatial interrelations

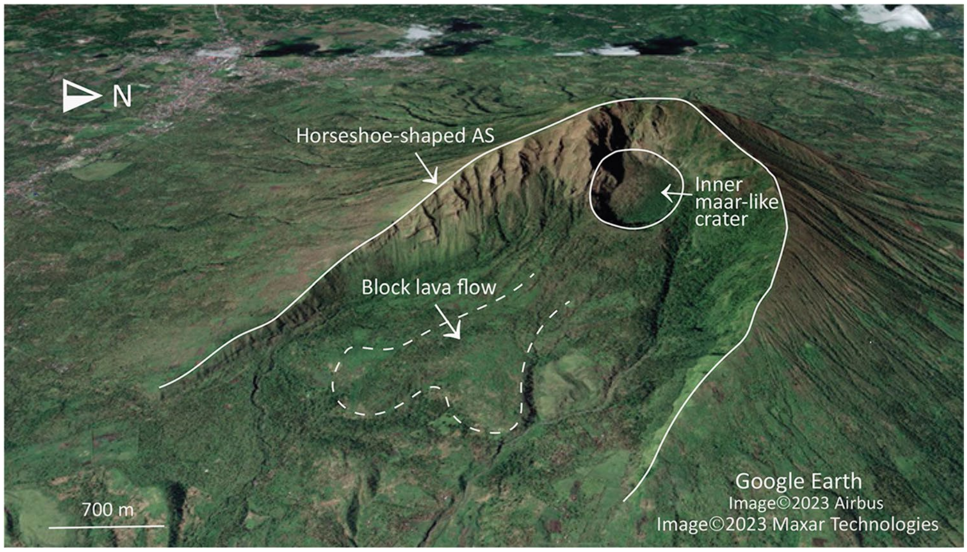

Fig. 3 Main geomorphological features of Iriga volcano: Buhi horseshoe-shaped avalanche scar and enclosed postcollapse volcanic landforms (block lava flow and maar-like crater)

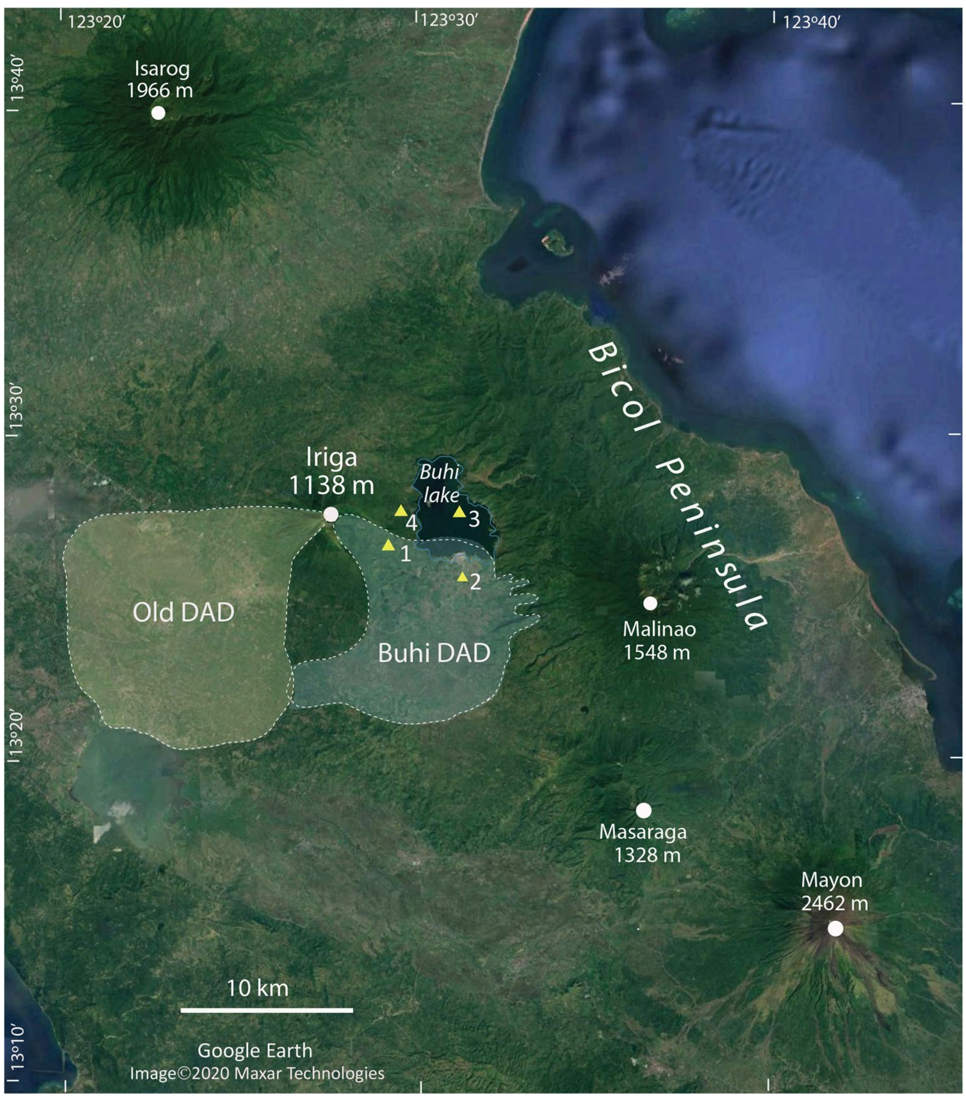

Fig. 4 Location of Iriga volcano with its two debris avalance deposits. Their limits are modified from Paguican et al. (2012). Sampling points (see Table 1) are indicated

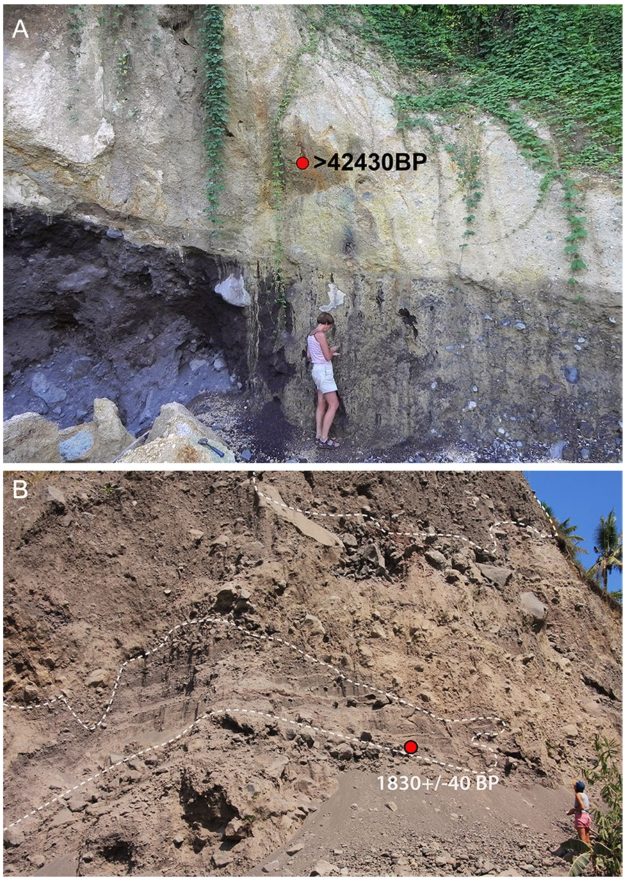

Fig. 5 ^{14}C-dated charcoal-bearing substrate material bulldozed and entrained by Buhi debris avalanche: **a** pumice-rich pyroclastic flow (> 42,430 BP) from sampling point 1, Fig. 4, and Table 1. **b** Blocks of basaltic-andesite scoria (dotted lines) with location of charred wood 1830 ± 40 BP from sampling point 2 (Fig. 4 and Table 1)

between the horseshoe-shaped Buhi avalanche scar, formed by the collapse, and the progressively superimposed younger volcanic landforms, as formed by the post-Buhi eruptions. This general scheme was then refined by stratigraphic investigations of the erupted products supplemented with ^{14}C AMS (accelerator mass spectrometer) radiocarbon dating method using the calibration database INTCAL09 (Reimer et al. 2009). It was performed by BETA Analytic's commercial radiocarbon laboratory, USA. In total, six samples were dated (two samples of paleosoil, two samples of lacustrine sediments, and two samples of charcoal contained in prehistoric pyroclastic deposits of Iriga (Table 1). These samples were collected at the points #1–4 (Fig. 4).

Determination of emplacement ages of Buhi DAD and products of the post-collapse eruptions

Most of the volcaniclastic deposits of Iriga, considered here, including those of the Buhi DAD, not contain organic material suitable for ^{14}C dating, which would directly provide emplacement ages. Thus, we determined ^{14}C ages of under- and over-laying organic-rich deposits (paleosoils, organic lacustrine sediments, and as well as charcoal-containing PDC units). The obtained pairs of pre- and post-^{14}C ages thus provided the lower and the upper age limits (the depositional time frames) of the deposit under or above which the sample was collected. ^{14}C dating of the overlying soil (of its oldest, lower part) commonly provides ^{14}C age that is several hundreds years younger than the actual emplacement age of the underlying volcaniclastic deposit (Scharpenseel and Schiffmann 1977). In contrast, dating of the underlying paleosoil or organic sediment provides the age value that closely

Table 1 Results of radiocarbon dating of volcanoclastic deposits, organic lake sediments, and soils of Mt. Iriga. See Fig. 4 for location of sampling points

Samples	Location (sampling point)	Coordinates	Dated deposits	Dated material/method	Conventional age, years BP	Calibrated age, years BP (2 sigma calibration)
Iriga1	Delafe quarry (point 1)	13°26′21.8″N 123°29′10.5″E	Pumice PF in DAD	Charred/radiometric	> 42,430	(Result is outside of the calibration range)
Iriga2	Buhi quarry (point 2)	13°25′13.4″N 123°31′10″E	Scoria PF in DAD	Charred/AMS	1830 + / − 40	1870–1640
Iriga3	Buhi lake (point 3)	13°27′16.0″N 123°30′53.7″E	Lowermost part of sediment core	Organic/AMS	1780 + / − 30	1810–1620
Iriga4	Buhi lake (point 3)	13°27′16.0″N 123°30′53.7″E	sediment core, below ash of phreatomagmatic eruption	Organic/AMS	1080 + / − 30	1060–930
Iriga5	Delafe quarry (point 1)	13°26′21.8″N 123°29′10.5″E	Paleosol between Buhi DAD and ash of phreatomagmatic eruption	Organic/AMS	1110 + / − 30	1070–950
Iriga6	Trail to crater (point 4)	13°27′16.4″N 123°29′24.1″E	Soil above pyroclasts of phreatomagmatic eruption	Organic/AMS	590 + / − 30	650–540

corresponds to the actual emplacement age of the overlying volcaniclastic deposit (Belousov et al. 2018). Thus, in cases where we obtained both pre- and post-^{14}C ages, we considered the ^{14}C age of the underlying paleosoil or organic sediment as emplacement age of the deposit, while the age obtained from the overlying soil was used to cross validate the emplacement age.

Coring of the bottom sediments of Buhi Lake

This coring was carried using a Livingstone-type drive rod piston corer (Livingstone 1955). Two lashed together fishing boats served as a coring platform. An echo sounder Lowrence Sea Charter with an integrated GPS unit was used to obtain water depth and geographical coordinates of the coring locations.

Water depth at the coring locations was up to 12 m. In total, six bottom sediment cores were collected with a maximum length of about 1 m. Several (up to 5) progressively deeper cores were obtained in each site in order to get a longer compound section of the sediment record as well as to try to reach the oldest sediment of the lake (i.e., as close as possible to the basal contact of the lake sediments and the inorganic substrate).

Youngest volcanic landforms of Iriga volcano

Horseshoe-shaped Buhi avalanche scar

Buhi scar is breached to the SE. The scar is 2 km wide and 3 km long, with nearly vertical walls up to 600 m high, enclosing a broad, flat crater floor up to 1.2 km wide. Two progressively younger, post-collapse volcanic structures, a block lava flow and a maar-like inner crater, are found within the scar (Fig. 3).

Block lava flow

It comprises two short flow lobes in the breach area of the avalanche scar. The source of the lava flow is located in the central-rear part of the Buhi avalanche scar (Fig. 3). Each lobe is about 1.5 km long and 50 m thick, with total flow volume about 0.02 km^3. The lava flow itself was not sampled and its petrographic and chemical composition is not known. The stubby morphology of the flow with its steep flow front indicates a high yield strength and evolved composition (Wadge and Lopes 1991).

Maar-like crater

It is 400 m across, 100 m deep, and is located in the source area of the lava flow, cutting its proximal part (Fig. 3). The crater is excavated by explosive activity into the underlying rocks, exposed in the nearly vertical wall of the crater. The crater is surrounded by a low profile pyroclastic apron composed of lithic-rich, cross-laminated, poorly sorted (2.5 phi) (*see* Supplementary Information *for the grain size data*) lapilli ash (Fig. 6a) containing cauliflower bombs. Ash particles are poorly vesicular and have blocky, angular shapes. The morphology of the crater, as well as lithological characteristics of the pyroclasts, indicates that they were ejected by a moderate-scale phreatomagmatic explosive eruption that produced base surges, ballistics, and ash fallout to form a maar-like crater. This eruption occurred after formation of the block lava flow and apparently represents the last and thus the youngest geologically detectable eruption of Iriga.

Age of the Buhi collapse and the following eruptions

Age of the Buhi collapse

No organic material was suitable for ^{14}C dating in the Buhi DAD. Thus, we determined ^{14}C emplacement ages of the older and younger deposits to constrain the depositional frames of the DAD (Table 1).

Pre-Buhi deposits

During emplacement, the Buhi debris avalanche incorporated a significant volume of the substrate materials, which are found as large (meters across) blocks of friable volcaniclastic deposits incorporated into the normal block facies of the Buhi DAD represented by fractured lava flows of the collapsed edifice. We dated fragments of charcoal in two different PF deposits, entrained in the DAD: a pumiceous PF with a ^{14}C age > 42,430 BP (Fig. 5a, Table 1) and St. Vincent-type PF of a scoriaceous basaltic andesite with a ^{14}C age of 1830 ± 40 BP (Fig. 5b, Table 1). The last date constrains the oldest limit of the Buhi DAD.

Probably the pumice PF was originally part of the relatively deep stratigraphy of the ring plane of Iriga. This deposit was probably exposed by faulting during gravitational spreading of the volcanic edifice that preceded the Buhi collapse (Paguican et al. 2012). The St. Vincent-type PF originally made up a superficial part of the pre-collapse ring plane stratigraphy. The Buhi avalanche traveled then over this ring-plane substrate.

Post-Buhi deposits

^{14}C dating of the lowermost part of organic-rich lacustrine sediment that accumulated in the Buhi lake after the

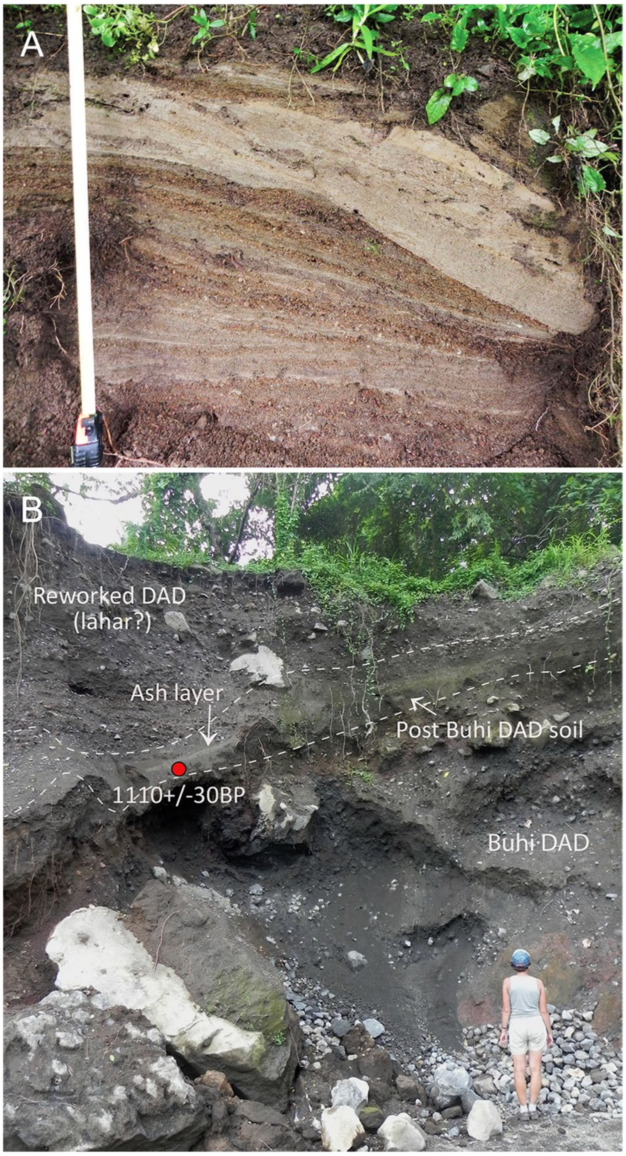

Fig. 6 Deposit of the post-Buhi phreatomagmatic eruption. **a** Base surges and fallout ash from sampling point 4 (Fig. 4 and Table 1). **b** Small quarry in block facies of Buhi DAD. Layer of ash fallout deposit of this eruption with thickness up to 6 cm is visible in the soil covering the DAD. ^{14}C age of the paleosoil below the ash is 1110 ± 30 BP. Sampling point 1 (Fig. 4 and Table 1)

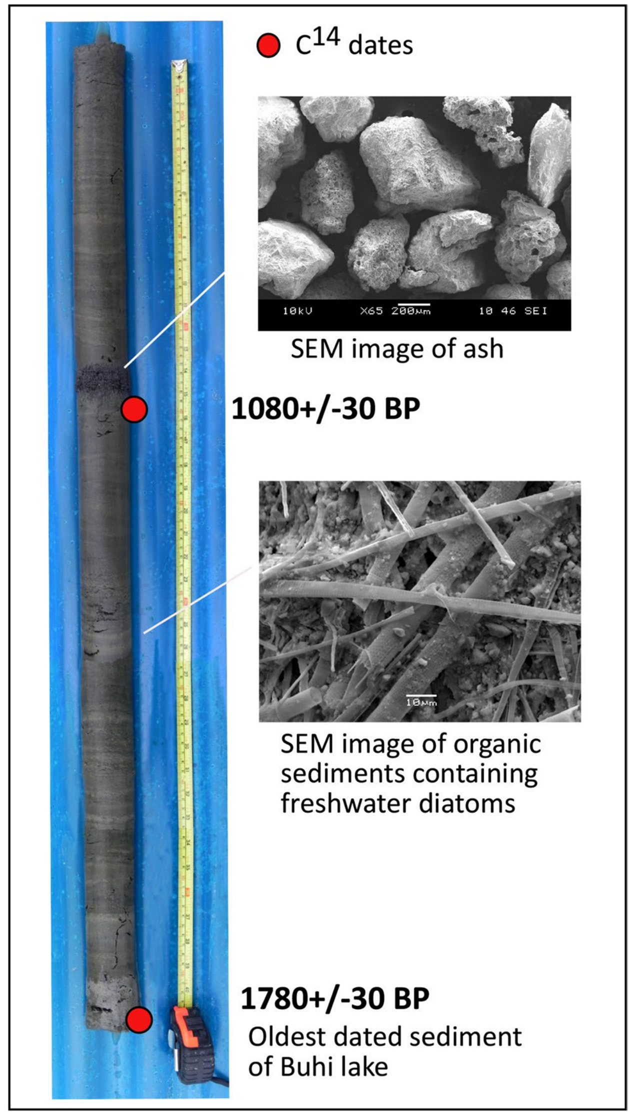

Fig. 7 Core of organic lake floor sediments of Buhi lake with ash layer from post-Buhi debris avalanche phreatomagmatic eruption. Length of the core 1 m, sampling point 3 (Fig. 4 and Table 1). Inserts show SEM images of the ash and the sediment

emplacement of the Buhi DAD provides an upper (youngest) limit to avalanche emplacement of 1780 ± 30 BP (Fig. 7, Table 1) (see *Stratigraphy of the cored lake sediments*). Hence, our ^{14}C ages indicate that the edifice collapse occurred sometime between 1780 and 1830 BP. Thus, the Buhi collapse turned out to be about 1400 years older than the age 1620 AD inferred by Aguila (1986) from historical reports of missionares of the area.

Age of the intra-scar maar-like crater

To constrain the age of the eruption that formed the maar-like crater, we dated the lowermost (oldest) part of the soil covering proximal base surge deposits associated with the phreatomagmatic eruption (Fig. 6a). This gives ^{14}C age of 590 ± 30 BP (Table 1). The paleosoil underlying distal ash of the same eruption found in locations where the paleosoil overlies the Buhi DAD (Fig. 6b) gives an age of 1110 ± 30 BP (Table 1). We consider the second age as the most likely estimate for the phreatomagmatic eruption and formation of maar-like crater inside the avalanche scar.

Stratigraphy of the cored lake sediments

Lakes are natural sediment traps that provide excellent conditions for preservation of ash fallout. To find ash layers relating to eruptions from Iriga following the Buhi collapse, we cored and investigated organic sediments accumulated in the Buhi Lake since its formation as a result of the emplacement of Buhi DAD.

The compound core of the retrieved lake sediments is about 1.67 m long. The core has an uppermost part that is 20–30 cm long and consists of gray, semi-liquid, homogeneous mud. This part probably represents modern sediment formed when shores of the lake became densely populated and cultivated. This surface layer of mud becomes more viscous with depth and over a length of 5–10 cm transforms into a greenish-gray peat-like material composed of compacted fine fibers of partly decayed lake algae. The sediment has fine parallel (varve-like) lamination 0.1–1 cm thick with diffuse contacts defined by slight variations of greenish and grayish colors. Some laminae are more prominent due to enrichment by freshwater diatoms (Fig. 7).

The compound sediment core contained only one layer of volcanic ash at a depth of about 104 cm from the modern water/sediment boundary. The layer is 2 cm thick, normally graded and composed of medium grained, poorly vesicular blocky particles (Fig. 7). Organic sediment directly below the ash layer provided a ^{14}C age of 1080 ± 30 BP (Table 1).

Organic sediment from the lowermost and thus deepest part of the core (65 cm below the ash layer) provided a ^{14}C age of 1780 ± 30 BP (Table 1). This age provides the upper age limit of the Buhi DAD emplacement. Despite several attempts to obtain deeper cores, the lake base was not reached. Based on the lower age limit of the DAD emplacement, considering the lake formation due to the emplacement of Buhi DAD 1830 ± 40 BP, and taking into account the average sedimentation rate in the lake of about 1 mm/year (calculated from the obtained ^{14}C ages of the sediment core), the coring nearly reached the lake base, being within few centimeters of it.

Discussion

Sequence and timing of the most recent eruptive events at Iriga

Structural relations of the youngest volcanic landforms of Mt. Iriga residing in the Buhi avalanche scar, as well as stratigraphic relationships of the corresponding volcaniclastic deposits of the volcano and supplemented by six new ^{14}C dates, allowed us to reconstruct the sequence and timing of the most recent eruptive events at Iriga (Fig. 8).

1. About 1830 ± 40 BP, Iriga produced a magmatic explosive eruption of St. Vincent type with the formation of an extensive scoriaceous PF of basaltic andesite that was emplaced at the SSE foot of the volcano. Volume of the erupted magma can be tentatively estimated as 0.01 km^3 DRE, making this VEI 3 event following Newhall and Self (1982).
2. The next event was a major flank collapse of Iriga to form the Buhi DAD. This occurred between 1830 ± 40 BP (the age of the first PF) and 1780 ± 30 BP (the age of the first organic sediment in the Buhi Lake, which formed as a result of the avalanche emplacement). The edifice col-

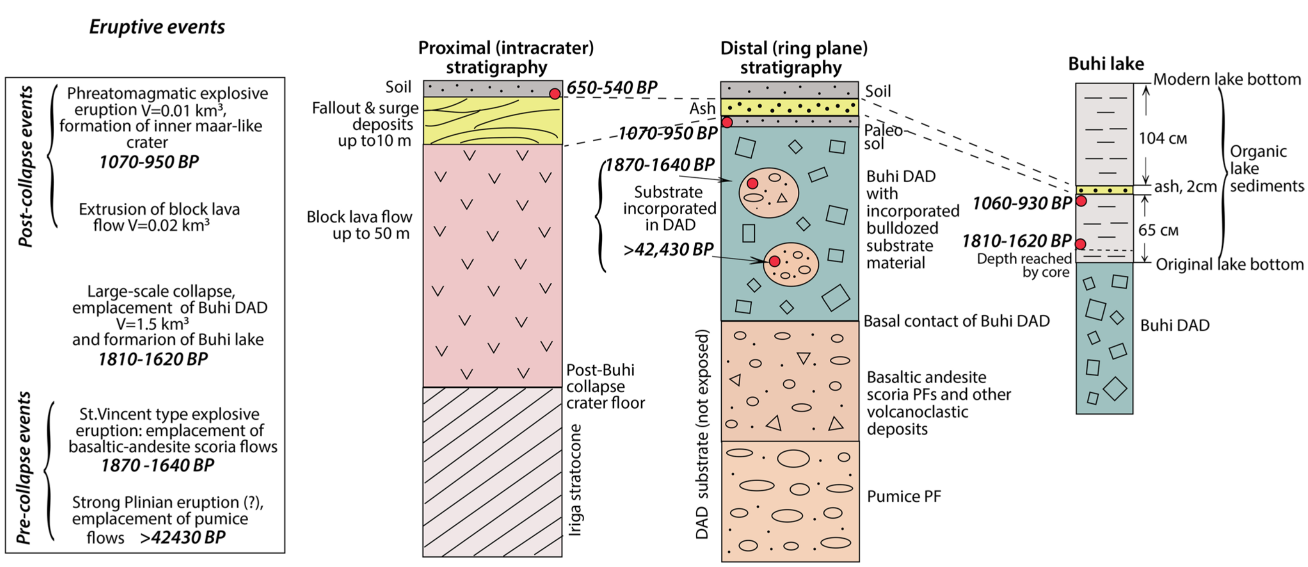

Fig. 8 Composite stratigraphic sections of Iriga volcano with proposed reconstructions of the eruptive events

lapse itself was not accompanied by, and did not provoke, any geologically detectable explosive eruption.

3. The first post-collapse magmatic eruption occurred no later than 700 years after the collapse, and definitely before 1110 ± 30 BP. This eruption extruded a small-volume (about 0.02 km^3) block lava flow in the central-rear part of the Buhi avalanche scar. In paleosoils covering the Buhi DAD, as well as in the cores of the Buhi Lake sediments, we found no pyroclastic material that could be associated with this eruption. Thus, we conclude that this extrusion was not accompanied by explosive activity strong enough to produce geologically identifiable pyroclastic deposits.
4. The next eruption of Iriga occurred at 1110 ± 30 BP. This eruption formed a small maar-like crater located inside the Buhi avalanche scar, in the vent area of block lava flow. This phreatomagmatic eruption produced base surges that affected inner parts of the Buhi avalanche scar. The accompanying ashfall formed a 2-cm-thick layer of ash in the sediments of Buhi Lake (Fig. 7). The volume of erupted magma probably did not exceed 0.01 km^3 (VEI 2–3). This eruption was the last, and youngest, eruption of Iriga that is recorded in the morphological features of the volcanic edifice and stratigraphic sequences of the area.

Possible trigger of the Buhi collapse and mechanisms of the post-collapse eruptions

The Buhi collapse of Iriga was preceded by gravitational spreading of the volcanic edifice (Paguican et al. 2012, 2014). Fresh deposits of scoriaceous basaltic andesite incorporated into the Buhi DAD indicate that the edifice collapse occurred about 50 years after a magmatic eruption of volcano with a date ~ 1830 BP. We hypothesize that the Buhi collapse could have been initiated by this eruption, which at first provoked a sluggish gravitational creep of the edifice, with spreading accelerated to develop into the full-scale failure and formation of the Buhi debris avalanche around 1780 BP. Similar "delayed" or "postponed" edifice collapse has been described at Popa volcano in Myanmar (Belousov et al. 2018). The collapse of Iriga was not immediately accompanied by explosive eruption, but < 700 years after the collapse (before ~ 1110 BP), a small-volume and highly viscous block lava flow was extruded at the head of the avalanche scar.

We suggest that this block lava flow was the result of eruption of residual magma that remained in the shallow magmatic system of Iriga after the ~ 1830 BP St. Vincent-type eruption. This remnant magma was degassed during the explosive event and was thus unable to vesiculate to produce an explosive eruption in response to the gravitational unloading. The unloading, however, caused this magma to slowly ascend to be erupted effusively no later than 700 years after the collapse event.

The subsequent ~ 1110 BP explosive eruption was probably associated with the first batch of new magma that ascended to the surface after the collapse event. This eruption was moderately explosive and phreatomagmatic, thus involving fragmentation due to interaction with groundwater. The horseshoe-shaped avalanche scar was a wet environment, being a closed water catchment where rocks, owing to humid, tropical climate, were saturated with groundwater.

These two eruptions (the block lava extrusion and the following phreatomagmatic explosive event) were the sole eruptions of Iriga occured after the Buhi collapse. Together with the pre-collapse St. Vincent-type eruption ~ 1830 BP, they comprise the entire eruptive activity of Iriga during the Late Holocene (i.e., over the last 2000 years) (Fig. 8) with this active volcano having been dormant since ~ 1110 BP. Modern activity of Iriga has been characterized by a relatively low rate of magma production since the gravitational collapse. This is unlike large-scale edifice collapses at many other volcanoes of the world, where large scale collapses lead to VEI 4–5 eruptions of high magnitude and intensity as, for example, at Mount St. Helens (Newhall and Self 1982). Instead the large-scale collapse at Iriga led to a just subtle intensification in eruptive activity in response to the landslide-induced gravitational unloading. The total volume of magma erupted by the volcano during last 2000 years is just 0.025 km^3 DRE at a low rate of magma production (about 0.01 km^3/millennium). This has been erupted as rare, weak-to-moderate scale (VEI 1–3) eruptions. Future eruptions most likely will be moderately explosive magmatic or phreatomagmatic, similar to the ~ 1830 and ~ 1110 BP eruptions. These eruptions can produce pyroclastic density currents of various types, posing hazards inside the Buhi crater and across the SE sector of the volcano. Extrusions of viscous lava flows or domes are also possible.

Conclusions

Our reconstructed eruptive history of Mt. Iriga shows that large-scale volcanic collapses can be provoked by eruptive magmatic activity that occurs not only immediately before the collapse but also by eruptions occurring several decades before collapse. In such cases the triggering event first initiates slow gravitational spreading (creep) of the edifice, which only after some time (several decades in our case) accelerates and evolves into full-scale edifice collapse with formation of debris avalanche. A similar sequence of events was reconstructed for large-scale collapse of Mt. Popa in Myanmar (Belousov et al. 2018), so the delayed or postponed collapse of Iriga is not unique. Thus, any magmatic eruption of a gravitationally unstable stratovolcano should be considered potentially collapsogenic, so that post-eruption monitoring of the edifice deformations is a valuable tool to forecast delayed large-scale collapses.

The first post-collapse eruption of Iriga volcano formed a block lava flow. We suggest that this lava flow was fed by magma remaining in the system after the pre-collapse eruption, that was the St. Vincent-type eruption of ~ 1800 BP. However, the source of the extrusive event still needs to be confirmed by petrological study such as the lava flow was not sampled due to poor exposure because of cover by dense rain forest.

The most significant pyroclastic deposit of Iriga is represented by a nonwelded pumice pyroclastic flow with ^{14}C age > 42,430 BP, found only as big blocks of substrate incorporated into the Buhi DAD (Fig. 5a). The source, volume, and other characteristics of the PF are unknown. Definitely the deposit of the pumice PF as well as its parental eruption is not typical for Iriga. This deposit could be associated with some unique event in eruptive history of the volcano, possibly with its ancient, pre-Buhi edifice collapse. Clarification of the origin of this PF is a goal for future geological research of the area.

Supplementary Information The online version contains supplementary material available at https://doi.org/10.1007/s00445-023-01653-0.

Acknowledgements The suggestions of handling editor Judy Fierstein, reviewer Lucia Capra, anonymous reviewer, and executive editor Andrew Harris were very helpful.

Funding Funding for the field works at Iriga volcano in 2010–2011 as well as for radiocarbon dating was provided by Earth Observatory of Singapore (Nanyang Technological University) where Belousovs worked under generous supervision of Chris Newhall.

References

Aguila LG (1986) Reconnaissance geology of large debris avalanche from Iriga volcano, Philippines. Phil Jour Volcanol 3:54–72

Beget J, Kienle J (1992) Cyclic formation of debris avalanches at Mount St. Augustine Volcano. Nature 356:701–704. https://doi.org/10.1038/356701a0

Belousov A, Belousova M, Voight B (1999) Multiple edifice failures, debris avalanches and associated eruptions in the Holocene history of Shiveluch volcano, Kamchatka, Russia. Bull Volcanol 61:324–342. https://doi.org/10.1007/s004450050300

Belousov A, Voight B, Belousova M (2007) Directed blasts and blast-currents: a comparison of the Bezymianny 1956, Mount St Helens 1980, and Soufriere Hills, Montserrat 1997 eruptions and deposits. Bull Volcanol 69:701–740. https://doi.org/10.1007/s00445-006-0109-y

Belousov A, Belousova M, Hoblitt R, Patia H (2020) The 1951 eruption of Mount Lamington, Papua New Guinea: devastating directed blast triggered by small-scale edifice failure. J Volcanol Geotherm Res 401:106947. https://doi.org/10.1016/j.jvolgeores.2020.106947

Belousov A, Belousova M, Zaw Khin, Streck MJ, Bindeman I, Meffre S, Vasconcelos P (2018) Holocene eruptions of Mt. Popa, Myanmar: volcanological evidence of the ongoing subduction of Indian Plate along Arakan Trench. J Volcanol Geotherm Res 360:126–38. https://doi.org/10.1016/j.jvolgeores.2018.06.010

Delcamp A, Roberti G, van Wyk de Vries B (2016) Water in volcanoes: evolution, storage and rapid release during landslides. Bull Volcanol 78(12):1–12. https://doi.org/10.1007/s00445-016-1082-8

DuFrane SA, Asmerom Y, Mukasa SB, Morris JD, Dreyer BM (2006) Subduction and melting processes inferred from U-series, Sr–Nd–Pb isotope, and trace element data, Bicol and Bataan arcs, Philippines. Geochim Cosmochim Acta 70(13):3401–3420. https://doi.org/10.1016/j.gca.2006.04.020

Dufresne A, Siebert L, Bernard B (2021) Distribution and geometric parameters of volcanic debris avalanche deposits. In: Roverato M, Dufresne A, Procter J (eds) Volcanic debris avalanches: from collapse to hazard. Springer, pp 75–90. https://doi.org/10.1007/978-3-030-57411-6_4

Eichelberger JC (2006) Volcanic edifice collapse and eruption response: a window on magma transport in the crust. AGU Fall Meet Abstr 2006:V24A-02

Glicken H (1996) Rockslide-debris avalanche of May 18, 1980, Mount St Helens Volcano, Washington. US Geological Survey. Open File Rep 96–677:98

Livingstone DA (1955) A lightweight piston sampler for lake deposits. Ecology 36(1):137–139

Nakamura Y, Glicken H (1988) Blast and debris-avalanche deposits of the 1888 eruption, Bandai volcano. J Geogr 97(4):309–316

Newhall CG, Self S (1982) The volcanic explosivity index (VEI) an estimate of explosive magnitude for historical volcanism. J Geoph Res: Oceans 87(C2):1231–1238

Paguican EMR, van Wyk de Vries B, Lagmay AMF (2012) Volcano-tectonic controls and emplacement kinematics of the Iriga debris avalanches (Philippines). Bull Volcanol 74(9):2067–2081. https://doi.org/10.1007/s00445-012-0652-7

Paguican EMR, Wyk V, de Vries B, Lagmay AM (2014) Hummocks: how they form and how they evolve in rockslide-debris avalanches. Landslides 11:67–80. https://doi.org/10.1007/s10346-012-0368-y

Pasquaré FA, Tibaldi A (2003) Do transcurrent faults guide volcano growth? The case of NW Bicol Volcanic Arc, Luzon, Philippines. Terra Nova 15(3):204–212. https://doi.org/10.1046/j.1365-3121.2003.00484.x

Reimer PJ, Baillie MG, Bard E, Bayliss A, Beck JW, Blackwell PG, Ramsey CB, Buck CE, Burr GS, Edwards RL, Friedrich M (2009) IntCal09 and Marine09 radiocarbon age calibration curves, 0–50,000 years cal BP. Radiocarbon 51(4):1111–1150

Scharpenseel HW, Schiffmann H (1977) Radiocarbon dating of soils, a review. J Plant Nutr Soil Sci 140(2):159–174

Siebert L (1984) Large volcanic debris avalanches: characteristics of source areas, deposits, and associated eruptions. J Volcanol Geotherm Res 22(3–4):163–197. https://doi.org/10.1016/0377-0273(84)90002-7

Siebert L, Roverato M (2021) A historical perspective on lateral collapse and volcanic debris avalanches. In: Roverato M, Dufresne

A, Procter J (eds) Volcanic debris avalanches: from collapse to hazard. Springer, pp 11–50
Ui T (1983) Volcanic dry avalanche deposits—identification and comparison with nonvolcanic debris stream deposits. J Volcanol Geotherm Res 18(1–4):135–150. https://doi.org/10.1016/0377-0273(83)90006-9
Ui T, Yamamoto H, Suzuki-Kamata K (1986) Characterization of debris avalanche deposits in Japan. J Volcanol Geotherm Res 29(1–4):231–243. https://doi.org/10.1016/0377-0273(86)90046-6
Voight B, Glicken H, Janda RJ, Douglas PM (1981) Catastrophic rockslide avalanche of May 18. In: Lipman PW, Mullineaux DR (eds) The 1980 eruptions of Mount St. Helens, Washington, vol 1250. US Geol Surv Prof Pap, pp 347–377
Voight B, Komorowski JC, Norton GE, Belousov AB, Belousova MG, Boudon G, Fransis PW, Franz W, Heinrich P, Sparks RSJ, Young SR (2002) The 26 December (Boxing Day) 1997 sector collapse and debris avalanche. In: Druitt TH, Kokelaar BP (eds) The eruption of Soufriere Hills Volcano, Montserrat, from 1995 to 1999. Geological Society, London, Memoirs 21:363–407
Wadge G, Lopes RMC (1991) The lobes of lava flows on Earth and Olympus Mons, Mars. Bull Volcanol 54:10–24
Watt S (2019) The evolution of volcanic systems following sector collapse. J Volcanol Geotherm Res 384:280–303. https://doi.org/10.1016/j.jvolgeores.2019.05.012
Wright HE (1967) A square-rod piston sampler for lake sediments. J Sediment Res 37(3):975–976
Yoshida H (2013) Decrease of size of hummocks with downstream distance in the rockslide-debris avalanche deposit at Iriga volcano, Philippines: similarities with Japanese avalanches. Landslides 10(5):665–672. https://doi.org/10.1007/s10346-013-0414-4